Generation of 3D polycrystalline microstructures with a conditioned Laguerre-Voronoi tessellation technique

Simone Falco[a], Jiawei Jiang[b], Francesco De Cola[a], Nik Petrinic[a]

[a] *Department of Engineering Science, University of Oxford, Parks Road, OX1 3PJ, Oxford, UK*
[b] *Department of Materials, University of Oxford, Parks Road, OX1 3PH, Oxford, UK*

Abstract

Voronoi tessellation techniques are widely accepted methods for the generation of representative models of polycrystalline microstructures of metallurgic and ceramic materials. Contrary to most of the Voronoi-based tessellation methods developed, the Laguerre Voronoi technique provides control over the size and shape of the cells, therefore allowing to simulate accurately the grain structure of a wide range of materials. This paper presents a method for the generation of numerical models of 3D polycrystalline microstructures, based on the Laguerre-Voronoi tessellation technique. An innovative approach to define the additional parameters required by the Laguerre-Voronoi formulation for the generation of realistic 3D microstructures is presented, providing the algorithm with information on the given microstructure from a set of 2D micrographs easily obtainable experimentally. The method implemented efficiently avoids *degenerated* cells (affecting the quality of the final structure) and finds the most representative set of input values by comparing 2D sections of the numerical model against 2D imaging of real polished surfaces. In this paper, the capability of the method developed is verified by reproducing the microstructure of polycrystalline alumina with various ranges of grain sizes, deriving from different sintering procedures.

Keywords: Polycrystalline materials, Grain structure reconstruction,

*Corresponding author
Email address: simone.falco@eng.ox.ac.uk (Simone Falco)

Laguerre-Voronoi tessellation, Scanning electron microscopy, Serial sectioning

1. Introduction

The ability to accurately reproduce microstructural features is fundamental for the correct simulation of the micro-mechanical behaviour of polycrystalline materials. Therefore, numerical models which are not representative of the real microstructures will lead to incorrect prediction of both global and local phenomena. This is particularly important in brittle materials, whose failure is dominated by crack propagation mechanisms that are strongly dependent on the local geometric and physical phenomena, such as the location of grain boundaries, triple points, crystallographic misorientation and crack initiation.

Several techniques have been developed for the generation of 3D models of polycrystalline microstructures, based on both experimental measurements and numerical approaches. All algorithms for the generation of geometrically and physically representative 3D models of polycrystalline microstructures rely upon a variety of experimental techniques of *non-destructive* and *destructive* nature.

Within the first category, X-ray (micro-) diffraction microscopy provides 3D microstructural representations of a wide range of polycrystalline materials [1, 2].

The destructive techniques are based on the interpolation of 2D images to reconstruct the 3D topology of the grain structure. A widely used technique is the "focused ion beam scanning electron microscope" (FIB-SEM), which consists of sectioning the material at given intervals taking SEM images of each surface [3].

The main disadvantage of the techniques based on the scanning of serial sectioned surfaces is the complex and time-consuming post processing required to analyse the amount of data produced. Moreover, the procedure might lead to non-unique topologies with apparent un-physical features (e.g. grain overlapping) in the reconstructed structure. However, in the recent years, the introduction of automated techniques (e.g. Robo-Met3D [4]) has reduced the

computational cost and time of the procedure.

The algorithms for the generation of 3D models from the experimental data acquired can be divided in two main groups: the *specific* aiming to reconstruct the particular microstructure under consideration, and the *generic* aiming to construct statistically representative microstructures. The former methods normally require very large amount of data and, if relying upon the destructive data acquisition methods, cannot furbish simulations of the mechanical response that can be compared against experiments since the specific sample was destroyed during data acquisition on the microstructure itself. The latter approach is more versatile, as it allows for sensitivity studies of the behaviour of the material upon the variation in its microstructural properties, including the ability to compare the results of thus furbished simulations against corresponding experiments on samples which did not need to be assessed explicitly.

Several such generic numerical generation techniques developed over the years exhibit considerably different levels of accuracy in representing the materials under consideration.

The methods based on regular morphologies (e.g. cubes [5], dodecahedra [6], truncated octahedra [7]) have the advantage of a low computational cost for both the generation and the further spatial discretisation (i.e. meshing) of the grains. The simplicity of these methods is counterbalanced by their inability to reproduce the variability in shape and size of the grains, which makes them unable to simulate localised phenomena.

Voronoi tessellation, and its variants, provide an analytical formulation able to reproduce the non-regularity of polycrystalline morphologies. Additionally, the straight edges and the planar faces of the grains are advantageous for further spatial discretisation [8].

More complex methods, able to reproduce irregular morphologies by simulating the grain-growth kinetics, have also been developed (e.g. Montecarlo-Potts [9], Phase-Field [10], Surface Evolver [11]), but their complexity and high computational cost, restrict their use to simulate actual grain growth mechanisms.

Voronoi tessellations have dominated the modelling of metallurgic and ce-

ramic microstructures in the recent decades because of the combination of the simplicity of formulation and the high representativeness of the results.

Among the several variation of the Voronoi tessellation algorithm available in the open literature, Poisson-Voronoi, Hardcore-Voronoi, and Laguerre-Voronoi formulations are widely accepted to generate tessellations statistically representative of real polycrystalline microstructures. Whilst the first two variants offer only a limited control over the shape and size of the cells, the Laguerre-Voronoi method modifies more deeply the formulation of the tessellation by imposing constraints on the initial state [12], thus allowing to model a wider range of grain structures (e.g. metals [13], foams [14], granular matter [15]).

The increased modelling capability offered by the Laguerre-Voronoi tessellation, however, comes at the cost of a non-bijective relation between the nuclei and the cells, for which a conditioning method is needed.

In this paper, the improvement offered by the implementation of the Laguerre-Voronoi tessellation, expressed in terms of representativeness of the microstructurals models generated, is illustrated. A novel methodology for the conditioning of the nuclei seeding procedure, to prevent the occurrence of *degenerated cells* within the structure, is implemented. The presence of many more degrees of freedom (i.e. weights) requires a technique for the extrapolation of the input parameters from experimental measurements. In particular, to illustrate the effectiveness of the proposed method, the approach presented in this paper relies solely upon the data collected from 2D SEM images of polycrystalline microstructures. The models generated using that data are then analysed using virtual serial-sectioning in order to generate 2D data for direct comparison against the SEM micrographs of the materials under consideration. Finally, a method to optimise the input of the Laguerre-Voronoi tessellation (i.e. weights) is described, showing the excellent agreement reached between numerical and experimental results.

2. Voronoi-based tessellation algorithms

Among the numerical techniques developed to generate representative models of polycrystalline microstructures, the Voronoi tessellation techniques are generally considered to offer an excellent compromise between representativeness and simplicity of formulation.

In this section, first the classic formulation is illustrated, highlighting its limits in representing real polycrystalline microstructures, then the methodology developed to reproduce experimental measurements, based on the Laguerre-Voronoi modification, is presented.

2.1. Formulation of the Voronoi tessellation

Given a finite set of N *nuclei* arbitrarily positioned in the space $\Re^3$, the Voronoi tessellation decomposes the three-dimensional space into one *cell* per each nucleus, consisting of all the points closer to the generating nucleus than to any other nucleus. Mathematically it can be expressed as:

$$\{R_{P_i}\} = \{x \in \Re^3 : ||\mathbf{P_i} - \mathbf{x}|| \leq ||\mathbf{P_j} - \mathbf{x}||\}\ j = 1, 2, ..., N : j \neq i \qquad (1)$$

where $\mathbf{P_j}$ is the position of the j-th nucleus, R_{P_i} is the cell associated to the nucleus $\mathbf{P_i}$, and $\mathbf{x}$ is the position of a generic point in $\Re^3$.

From this formulation, it is clear that the only control over the cell size and shape is given by imposing constraints on the nuclei seeding procedure. The *Poisson* [16] and *Hardcore* [17] constraints are arguably the most common additions to the Voronoi tessellation.

The Hardcore-Voronoi tessellation, in particular, has often being used to generate statistically representative models of metallurgic [17] and ceramic [18] polycrystalline microstructures, as well as of granular matter [19]. It offers the possibility to control the sphericity of the grains through the definition of a single scalar value: the *Hardcore radius* ρ, that represents the minimum distance between the nuclei during the seeding process. In 3D this operation

can be expressed as:

$$||\mathbf{P_i} - \mathbf{P_j}|| = \sqrt{\sum_{k=1}^{3} (P_{i_k} - P_{j_k})^2} > \rho \;\; \forall (i,j) = 1,2,...,N : j \neq i \tag{2}$$

The introduction of three more parameters allows for a certain degree of control over the shape of the grains, by defining a privileged growing direction of the cells (i.e. Extended Hardcore [18]).

However, the distribution of grain size of all the Voronoi assemblies based on constraints of the nuclei seeding exhibits a typical bell-shaped curve, as reported by [12], which is not necessarily representative of real granular materials.

In particular, they are not able to represent the wide range of real grain sizes and the presence of large grains within the microstructure, as illustrated in Section 3.

2.2. Laguerre-Voronoi tessellation

In place of the *Eulerian* distance used in the classic Voronoi formulation, the Laguerre-Voronoi tessellation introduces the so-called *power-distance*, defined as:

$$pow(\mathbf{x}, (\mathbf{P_i}, w_i)) = ||\mathbf{P_i} - \mathbf{x}||^2 - w_i \tag{3}$$

where $\mathbf{x}$ is the position of a generic point in $\Re^3$, $\mathbf{P_i}$ the position of the generic i-th nucleus, and w_i the weight associated to it. Note that, if all the weights are equal, the power distance reduces to the Euclidean.

The boundary plane between two neighbouring nuclei is perpendicular to the line connecting them and consists of all the points $\mathbf{x}$ such that:

$$\mathbf{x} \in \Re^3 : 2\langle \mathbf{x}, \mathbf{P_i} - \mathbf{P_j} \rangle = ||\mathbf{P_i}||^2 - ||\mathbf{P_j}||^2 + w_j - w_i \tag{4}$$

Clearly, the definition of *"neighbouring"* grains is different from the one based on the minimum distance between nuclei used in the classic Voronoi approach, and it requires the used of a *weighted* distance. For the work presented in this paper, this distance is performed using TetGen libraries [20].

If all the weights are positive, they can be interpreted as the square of the radius of spheres centred in the corresponding nuclei (i.e. $r_i = \sqrt{w_i}$). It is

worth highlighting that the assumption of adopting only positive values for w_i is not reducing the generality of the approach, since Eq. 4 indicates that the tessellation remains identical if the same constant value is added to all the weights [21].

The adoption of the geometrical similarity allows to write the formulation of the Laguerre-Voronoi tessellation as:

$$\{R_{P_i}\} = \{x \in \Re^3 : ||\mathbf{P_i} - \mathbf{x}|| - r_i^2 \leq ||\mathbf{P_j} - \mathbf{x}|| - r_j^2\}\ j = 1, 2, ..., N : j \neq i \quad (5)$$

From the increased control over the outcome of the tessellation, with respect to the classic Voronoi formulation, due to the addition of many degrees of freedom (i.e. the weights of the nuclei), derive the non-univocal relation between cells and nuclei, which can hinder the quality of the resulting numerical models. In particular the following *degenerated* conditions can occur:

- Cells do not necessarily contain their corresponding nuclei;
- Cells might contain multiple (or none) nuclei;
- Not every nuclei necessarily generate a cell.

which affect the quality of the final tessellation, and hinders the further discretisation procedure required to generate FE (Finite Elements) models of the structure.

Visual examples of the appearance of these three conditions are reported in Figure 1.

In particular, the 2D illustration presents all three degeneracies described, with the cell i not containing its nucleus P_i, the cell j containing multiples nuclei, and the nucleus P_k not generating any cell.

From the examples, as well as from the mathematical description of the tessellation, appears that the occurrence of the undesired cells can be avoided by imposing a non-overlapping condition on the spheres representing the weights of the nuclei. Therefore, to assure that every nucleus generates a cell, and lies within it, an innovative method for efficiently generate dense packing of spheres is adopted, as presented in the next section.

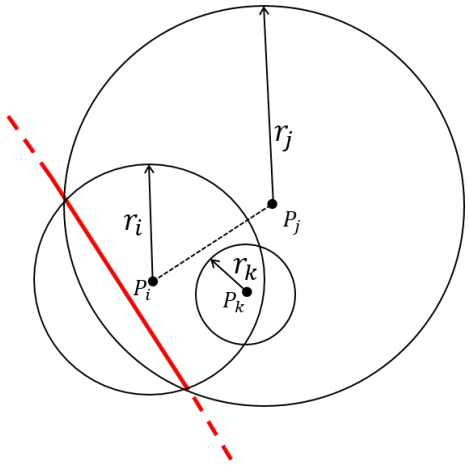

Figure 1: Illustration of a grain boundary (red line) between cell i (left) and cell j (right) generated by the nuclei P_i and P_j

2.3. Conditioning method for the nuclei seeding

Random sequential positioning of balls is often used as conditioning method [22, 23]. Whilst appealing for the simplicity of formulation, the computational cost of this method increases hugely with the density of the packing. Nevertheless, a loose assembly of spheres generates a wide variability in the tessellation properties (being the weights equal), which might reduce the representativeness of the numerical models of the polycrystalline microstructures.

For these reasons, the conditioning method adopted in this paper generates dense three-dimensional packing of spheres with an arbitrary radii distribution, based exclusively on tangency conditions, and is an adaptation of the *3D-clew* packing algorithm developed by the authors, and presented in [24].

The method consists of placing the spheres, with radii equal to the square root of the weight, following a three-dimensional spiral pattern. The origin of the local coordinate system is defined as the centre of the first sphere (i.e. *central*), whilst the position of the centre of the second sphere, tangent to the central one, defines the direction of the X axis. Each of the subsequent spheres is added imposing its tangency both to the central and to the sphere previously

inserted, as represented in Figure 2.

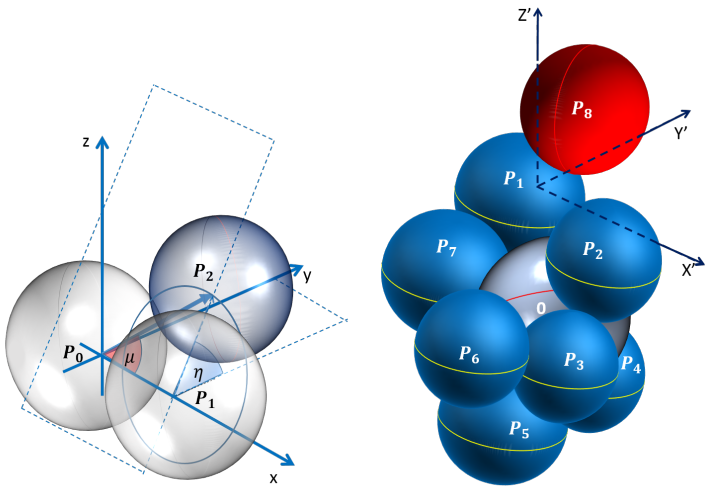

Figure 2: Illustration of the tangency condition (left), and the positioning of a sphere (red) around a new central one (right)

The tangency condition only defines the value of the angle μ_j in Figure 2, as:

$$\mu_j = \cos^{-1}\left[\frac{r_0^2 + r_i \cdot r_0 + r_0 \cdot r_j - r_i \cdot r_j}{(r_0 + r_i) \cdot (r_0 + r_j)}\right] \tag{6}$$

where r_0, r_i, and r_j are, respectively, the radius of the central, the previous, and the current sphere, reported respectively as P_0, P_1, and P_2 in Figure 2 (left). The angle η, instead, is assigned randomly.

The possible overlapping of the newly added sphere with any of the previously added is checked by evaluating the distance between their entres, and if any overlap is detected, the sphere is incrementally translated along the blue circle Figure 2 (i.e. varying η whilst keeping μ constant). If no value of η can be found to generate a sphere not overlapping with any of the previous ones, the central sphere is considered to be *saturated*, and the second sphere is imposed as the new central, as illustrated in Figure 2 (right).

The algorithm developed can then generate random geometrical packing of non-overlapping spheres with arbitrary radii distribution by iterating the

procedure described in this section. The position of the centres of the spheres in the obtained assembly and the relative radii are then used as coordinates and weights of the nuclei for the Laguerre-Voronoi tessellation.

An example of the conditioning spheres and the relative tessellation is reported in Figure 3.

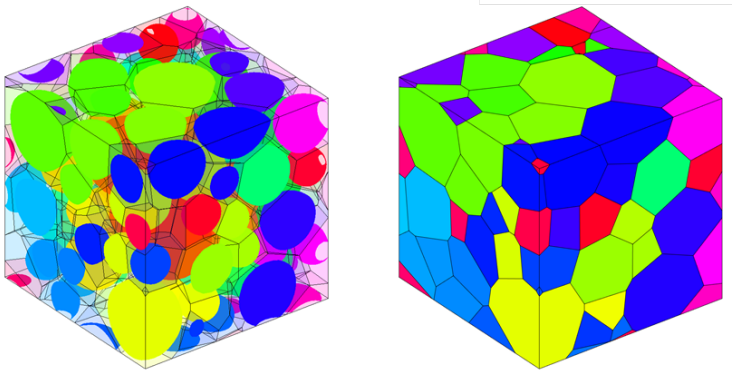

Figure 3: Packing of conditioning spheres (left) and relative Laguerre-Voronoi tessellation (right)

2.4. Serial sectioning of the numerical model

To assess the quality of the models generated, the numerical results are validated against experimental measurements. Given the complexity of the experimental reconstruction of 3D polycrystalline microstructures, the validation approach presented in this paper is based on the use of 2D imaging of the microstructure. In particular, SEM images of polished surface of the material are used to measure the area of each grain, as presented in Section 3.

To directly compare the numerical model against the 2D images of the microstructure, a virtual serial-sectioning of the cells is performed. Therefore, after having eliminated the cells generated from the outer layer of nuclei (to avoid unbounded cells and boundary influence) the structure is *sectioned* along parallel planes, producing 2D models directly comparable against the experimental SEM images, as illustrated in Figure 4.

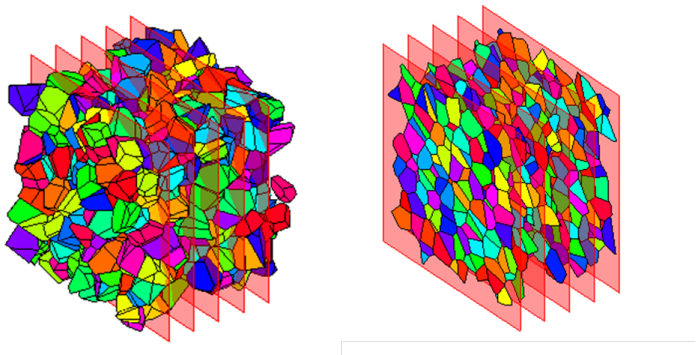

Figure 4: Serial sectioning of a 3D structure with 5 planes (left), and relative 2D projections (right)

The method adopted in this paper for the sectioning of the structure, based on the algorithm for the shaping of numerical models of polycrystalline microstructures developed by the authors [18], mimics the outcome of real cutting procedures by cropping the cells along arbitrarily oriented planes. The procedure to crop a single cell along an arbitrarily oriented plane can be outlined as follows: (i) detect the nodes beyond the cropping plane; (ii) find the intersect of the cell edges connected to the *external* nodes with the cropping plane; (iii) create the new face with the nodes laying on the cropping plane. An illustration of the procedure is presented in Figure 5.

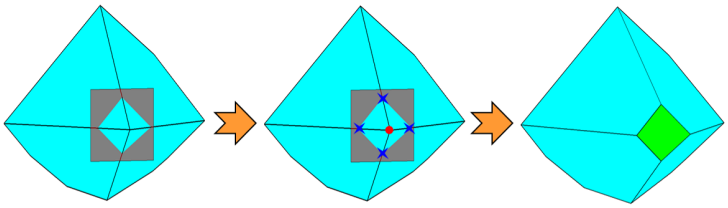

Figure 5: Cropping of a cell along a plane: The *external* node (red circle) is replaced by the intersections of the cell edges with the plane (blue crosses), and a new face (green) is created

By repeating the procedure for all the cells, the 2D section of the structure along a plane is generated.

2.5. Computational cost and scalability

The computational cost of the procedure can be evaluated as the sum of the costs of the two main operations: *geometrical packing of spheres* and *generation of the Laguerre-Voronoi cells*.

The high efficiency of the methods implemented guarantees a reduced computational cost for the generation of the structure, thus allowing the optimisation procedure presented in Section 4.2. The use of a geometrical algorithm for the packing of the spheres based on tangency, instead of a random deposition method, has the double advantage of avoiding computationally expensive trial-and-error insertion of spheres, still producing dense assemblies. The reduced void ratio of the assembly is particularly important to ensure a close correspondence between the weight of the nuclei and the actual size of the cell, which guarantees a good representativeness of the models even using the 2D grain size measurements (as presented in Section 4.1), and therefore a reduction of the computational cost of the optimisation process.

Additionally, the computational advantage of the method developed is enhanced when using structures with high number of grains, due to the relatively small scalability factor. Specifically, the computational cost of the spheres packing algorithm have been proved to be between $O(n \log n)$ and $O(n^2)$ [24], where n is the number of spheres, whilst the generation of a 3D Voronoi tessellation has an estimated computational cost of $O(n \log v)$ [25], where v is the number of vertices in the tessellation.

3. Experimental measurements

The aforementioned complexity and limitations of the experimental approach for the reconstruction of 3D polycrystalline microstructures limit the use of experimental techniques for the generation of representative numerical models.

For this reason, the validation of the numerical results presented in this paper relies on the 2D images of polished surfaces obtained with SEM technique. The

equivalent grain size distribution is calculated from 2D SEM images, and it is used both as initial guess for the weight of the Laguerre-Voronoi tessellation and as validation of the numerical models generated.

In particular, the results presented refer to polycrystalline alumina (Al_2O_3), sintered from the same powder but at different temperatures. As it is widely known, the sintering temperature has a major influence on the final grain size distributions in ceramic materials. In particular, the specimens presented in this work show that the use of three different sintering temperatures (i.e. 1400°C, 1450°C, and 1500°C) generates structures with different grain sizes.

3.1. Sample manufacturing and imaging

The alumina specimens investigated in this study were sintered from as-received TM-DAR alumina powder ($\geq$99% purity, mean particle size $150nm$, Taimei Chemicals Co. Ltd. Tokyo, Japan) at three different temperatures: 1400°C, 1450°C, and 1500°C (all held for 1h, 5°C/min heating/cooling rate from/to room temperature in air) in a tube furnace.

To avoid possible distortion in the microstructure in the proximity of the surface of the samples the sintered specimens were sectioned with a diamond saw, and the cross sections were polished sequentially using Diamond Polish (Kemet) of different grades from $55\mu m$ to $1\mu m$.

The polished samples were, then, thermally etched in the same air furnace where they were sintered at temperatures of 50°C lower than their sintering temperature, for 18 minutes, to reveal grain boundaries, and finally sputter coated with a 3 nm thick layer of platinum to reduce the surface charging.

A total of 18 SEM images (6 per each material analysed) were taken at random positions on the treated surfaces. Given the scarce contrast in the SEM images, the grain boundaries were highlighted manually, and then digitalised using *imageJ* software [26], as shown in Figure 6.

3.2. Average grain size measurement

A simple technique to evaluate the average equivalent grain size $\bar{G}$ is the widely adopted Mendelson linear intercept method [27], which consists of count-

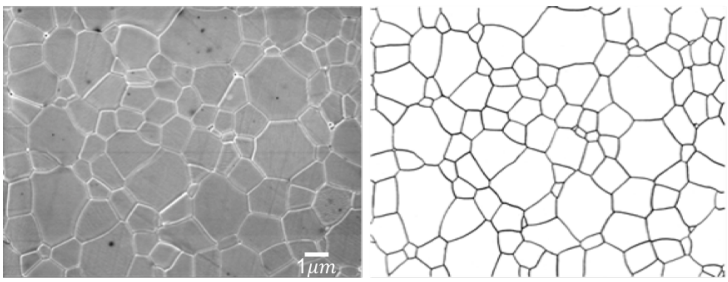

Figure 6: SEM image of the 1400°C alumina (left) and digitalisation of the grain boundaries (right)

ing the number of grain boundaries intercepted (N) by straight lines of total length L on SEM images with a magnification M, and can be expressed as:

$$\bar{G} = 1.56 \left(\frac{L}{MN} \right) \tag{7}$$

The correction factor equal to 1.56 is imposed to account for the three-dimensionality of the grains [28].

The relative density, with respect to the theoretical value for alumina ($3.98 g/cm^3$), and the mean grain size of the three materials considered in this paper is reported in Table 1.

Sintering temp [°C]	Etch temp [°C]	Relative density	$\bar{G}$ [μm]
1400	1350	99.9%	1.551 ± 0.029
1450	1400	100.4%	2.518 ± 0.104
1500	1450	99.8%	3.296 ± 0.096

Table 1: Average grain size obtained with the Mendelson linear intercept method on 2D SEM images

3.3. Particle analysis

The approach based on Mendelson intercept method, however, does not provide any information on the actual distribution of the equivalent grain size around the mean value.

The software *imageJ* was used to calculate the areas (A) of the internal grains (i.e. the grains intersecting the edges of the SEM images are ignored),

from which the equivalent grain size in 2D (g) is evaluated as:

$$g = \sqrt{\frac{4A}{\pi}} \tag{8}$$

The grain size measurements, based on the analysis of 6 SEM images for each of the 3 materials considered in the work presented in this paper are summarised in Figure 7.

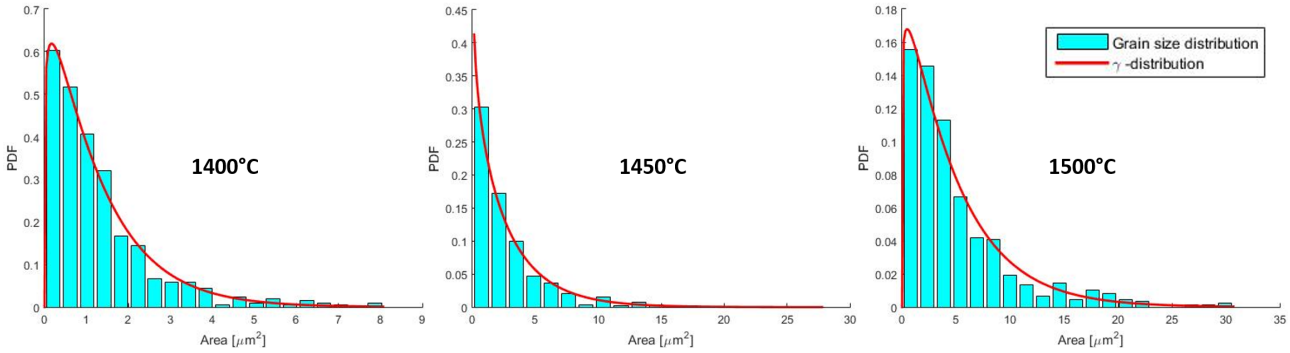

Figure 7: Histogram and γ distribution of experimentally measured grain areas

The bars in Figure 7 represent the *probability distribution function* (PDF) of the grain areas, whilst the red lines are the γ-PDF, which provide a good description of the size distribution by defining only two parameters κ and θ:

$$f(A;\kappa,\theta) = \frac{A^{\kappa-1}e^{\frac{A}{\theta}}}{\theta^{\kappa}\Gamma(\kappa)} \tag{9}$$

where Γ is defined as:

$$\Gamma(t) = \int_0^{\infty} x^{t-1}e^{-x}dx \tag{10}$$

The use of PDFs eliminates the dependence of the distribution on the sampling exhibited by the histogram representation.

Additionally, for each considered grain, ImageJ software provides the values of four *shape descriptors* - circularity (C), roundness (R), and aspect ratio (AR)

- defined respectively as:

$$C = \frac{4\pi A}{P} \qquad R = \frac{4A}{\pi d_{max}^2} \qquad AR = \frac{d_{min}}{d_{max}} \tag{11}$$

where P is the perimeter of the particle, and d_{max} and d_{min} are the values of the length of the major and minor axis of the fitting ellipse.

4. Results and Validation

Given the definition of the conditioning approach relying on the geometrical distribution of weights, the validation and optimisation of the experimental results are based on the grain size of the particles. Nevertheless, the effect on the shape factors is also reported for completeness.

4.1. Input of the Laguerre Voronoi tessellation

The values of the equivalent grain size distribution calculated from the experimental measurements are used as initial guess for the weight of the nuclei in the Laguerre-Voronoi tessellation.

The weights are divided in discrete bins of values, expressed as fraction of the maximum equivalent size measured for the specific material considered. The effect of the number of bins used (hereinafter referred to as N_w) is explored by using 3, 4, 5, and 6 unevenly spaced values of the weight for each material analysed.

In Figure 8 the γ-PDF of the results of 5 tessellations (consisting of about 100 grains each), obtained using the experimental equivalent radius distributions, are reported. The effect of N_w is illustrated by comparing four different unevenly spaced set of bins for the weights (w_i), expressed as fraction of the maximum equivalent radius measured experimentally.

The increase of N_w appears to reduce the difference between the numerical and the experimental distribution of 2D grain areas, thus improving the representativeness of the microstructural models generated, which for some configuration fall mostly within the experimental scatter represented by the grey area. Also, the comparison against the classic Voronoi tessellation shows the

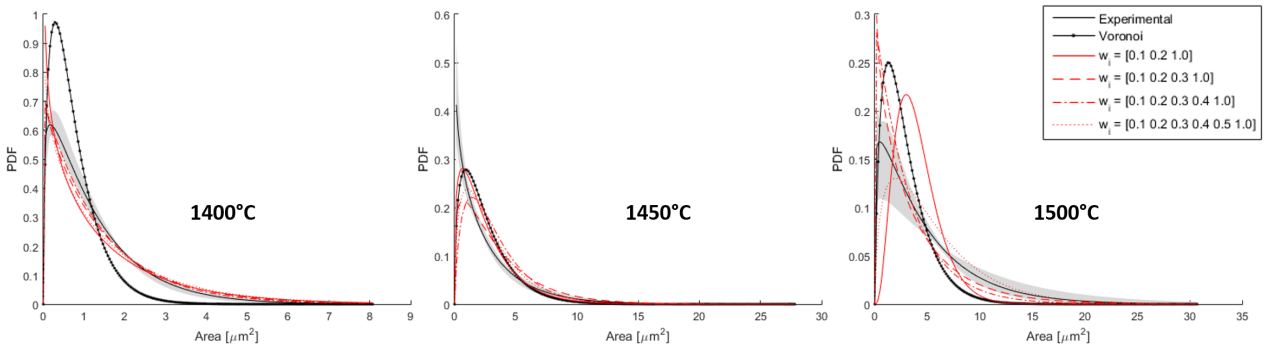

Figure 8: Comparison of grain size γ distributions of experimental measures and numerical models generate with classic Voronoi and Laguerre-Voronoi with different N_w

improvement of the Laguerre formulation in reproducing the presence of large grains in the structure.

To evaluate the representativeness of the numerical models, an error parameter ($\mathcal{O}$) is defined based on the quadratic deviation of the numerical PDF_n from the experimental PDF_e:

$$\mathcal{O} = \int_0^\infty \frac{[PDF_n(A) - PDF_e(A)]^2}{PDF_e(A)} dA \tag{12}$$

For the three materials analysed (identified by the sintering temperature), the error $\mathcal{O}$ for the classic Voronoi tessellation and of the Laguerre-Voronoi tessellations with different N_w are presented in Table 2.

Material	$\mathcal{O}(Voronoi)$	$\mathcal{O}(N_w = 3)$	$\mathcal{O}(N_w = 4)$	$\mathcal{O}(N_w = 5)$	$\mathcal{O}(N_w = 6)$
1400°C	0.2802	0.0845	0.0391	0.0162	0.0935
1450°C	0.2264	0.0528	0.0820	0.1583	0.0943
1500°C	0.3275	0.0676	0.0279	0.0931	0.0054

Table 2: Values of error for the different tessellation for the three materials analysed

In terms of grain size distribution, the adoption of the Laguerre-Voronoi tessellation proves to noticeably improve the representativeness of the numerical models with respect to the classic Voronoi tessellation.

The effect on the shape factors, instead, proves to be minimal. In partic-

ular, both the classic Voronoi and the Laguerre-Voronoi can reproduce quite accurately the mean value of both circularity and roundness (within 2% error), but they both overestimate the variance of the distribution. An higher error (within 10%), instead, is observed in the prediction of the aspect ratio, still with an higher variance of the distribution with respect to the experimental results.

The scarce influence of tessellation method introduced in this paper over the shape of the Voronoi cells generated is justifiable by the nature of the Laguerre-Voronoi approach, based exclusively on the alteration of the definition of distance.

4.2. Optimisation of the input values

Further improvement in the representativeness, in terms of grain size distribution, of the numerical models generated can be obtained optimising the value and the distribution of the weights assigned.

The non-univocal nature of the problem analysed (i.e. the same input values do not necessarily provide the same output tessellation) hinder the possibility of applying a gradient based optimisation [29] for the *fine-tuning* of the input values. Therefore, given the good quality of the initial guess from 2D measures, a *brute force* type method is adopted in this paper, which consists of keeping the number and the values of the weights constant, whilst imposing a finite number of variations ($2n_i + 1$) to the fraction of each assigned weight determined from the 2D measurements ($F^0_{w_i}$), and trying all the possible combinations.

In particular, given an arbitrarily assigned quantity δ, the vector of all the variations of the generic weight fraction F_{w_i} can be expressed as:

$$F_{w_i}(k) = F^0_{w_i} + (k - n_i - 1)(-1)^k \delta \quad \forall k = 1, 2, ..., (n_i + 1) \tag{13}$$

The total number of numerical models generated during the optimisation process is given by the permutation of the F_{w_i} for all the weights examined, which can be expressed mathematically as:

$$C_w = \prod_{i=1}^{N_w} (2n_i + 1) \tag{14}$$

Which, in case the number of variations is equal to n for all the $F^0_{w_i}$, reduces to $C_w = (2n+1)^{N_w}$. However, since the distributions exhibiting non-physical (i.e. negative) values of weight fraction F_{w_i} are neglected, the actual number of models generated can be smaller.

In particular, the optimisations presented in this paper use as input $n = 1$ and δ equal to 2.5 times the minimum initial proportion of weights.

The comparison of the result of the optimisation against the experimental measures is presented in Figure 9.

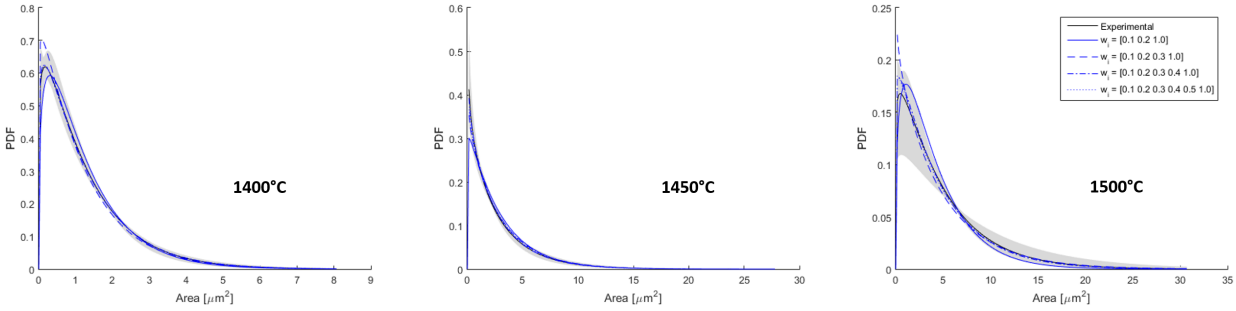

Figure 9: Comparison of γ distributions of experimental measures and optimised numerical models for different N_w

For all the combinations explored, the optimisation algorithm adopted is able to produce a distribution mostly within the statistical variation of the experimental values considered.

A quantitative validation of the numerical results, expressed in terms of error $\mathcal{O}$, is reported in Table 3, showing the excellent agreement achieved.

Material	$\mathcal{O}(N_w = 3)$	$\mathcal{O}(N_w = 4)$	$\mathcal{O}(N_w = 5)$	$\mathcal{O}(N_w = 6)$
1400°C	0.0073	0.0087	2.51E-4	1.98E-5
1450°C	0.0111	0.0043	8.59E-4	0.0019
1500°C	0.0401	0.0093	0.0028	0.0015

Table 3: Values of error for the different tessellation for the three materials analysed

The choice of the number of values for the input of the weights is a trade-off between the quality of the initial guess and the computational cost of the

optimisation algorithm.

5. Conclusions

This paper presents a method that, starting from 2D grain size measurements, generates numerical models of three-dimensional microstructures representative of real polycrystalline materials.

The distribution of 2D grain sizes, measured from SEM images of polished surfaces, is used as input for the weight of the 3D Laguerre-Voronoi tessellation. To avoid degenerated grains, deriving from the adoption of the power distance, a conditioning method for the seeding of the nuclei is implemented. Using the geometrical equivalence between the weight of a Laguerre-Voronoi cell and the square of the radius of a sphere centred in the respective nucleus, the seeding is performed using a geometrical sphere packing algorithm, based on the simultaneous tangency of at least three spheres.

The accuracy of the thus generated structures is validated against experimental measurements by comparing the distribution of grain areas of virtual sections of the numerical models against the ones measured from 2D SEM images of real alumina microstructures. The parametric study performed shows that, even using a reduced number of weights, the adoption of Laguerre-Voronoi tessellation provides significant improvement of the reproduction of realistic grain size distributions - without changing significantly the shape factors of the grains - with respect to the classic Voronoi tessellation. In particular, the ability to generate relatively large grains in the structure increases the representativeness of the numerical models, as proven by the validations presented.

Finally, to further increase the representativeness of the numerical models, an optimisation process is implemented. The *brute force* algorithm implemented explores a finite number of weight distributions around the initial value to find the best set of input values. The parametric study presented in the paper shows that the approach adopted allows to generate numerical models with grain size distribution within the experimental scatter, even for a reduced number of iterations.

Acknowledgement

The authors gratefully acknowledge the support of the United Kingdom Defense Science and Technology Laboratory (DSTL), Grant No: DSTL/AGR/00507/01.

[1] Poulsen HF. *Three-dimensional X-ray diffraction microscopy: mapping polycrystals and their dynamics*, vol. 205. Springer Science & Business Media, 2004.

[2] Wielewski E, Menasche D, Callahan P, Suter R. Three-dimensional α colony characterization and prior-β grain reconstruction of a lamellar ti–6al–4v specimen using near-field high-energy x-ray diffraction microscopy. *Journal of Applied Crystallography* 2015; **48**(4):1165–1171.

[3] Groeber M, Haley B, Uchic M, Dimiduk D, Ghosh S. 3d reconstruction and characterization of polycrystalline microstructures using a fibsem system. *Materials Characterization* 2006; **57**(45):259 – 273.

[4] Spowart JE. Automated serial sectioning for 3-d analysis of microstructures. *Scripta Materialia* 2006; **55**(1):5–10.

[5] Raabe D, Zhao Z, Mao W. On the dependence of in-grain subdivision and deformation texture of aluminum on grain interaction. *Acta Materialia* 2002; **50**(17):4379–4394.

[6] Zhao Z, Kuchnicki S, Radovitzky R, Cuitino A. Influence of in-grain mesh resolution on the prediction of deformation textures in fcc polycrystals by crystal plasticity fem. *Acta materialia* 2007; **55**(7):2361–2373.

[7] Jivkov A, Marrow T. Rates of intergranular environment assisted cracking in three-dimensional model microstructures. *Theoretical and Applied Fracture Mechanics* 2007; **48**(3):187–202.

[8] Aurenhammer F. Voronoi diagrams - a survey of fundamental geometric data structure. *ACM Computer Surveys* 1991; **23**(3).

[9] Zöllner D, Streitenberger P. Three-dimensional normal grain growth: Monte carlo potts model simulation and analytical mean field theory. *Scripta materialia* 2006; **54**(9):1697–1702.

[10] Krill Iii C, Chen LQ. Computer simulation of 3-d grain growth using a phase-field model. *Acta materialia* 2002; **50**(12):3059–3075.

[11] Wakai F, Enomoto N, Ogawa H. Three-dimensional microstructural evolution in ideal grain growthgeneral statistics. *Acta Materialia* 2000; **48**(6):1297 – 1311.

[12] Quey R, Dawson P, Barbe F. Large-scale 3d random polycrystals for the finite element method: Generation, meshing and remeshing. *Computer Methods in Applied Mechanics and Engineering* 2011; **200**(17):1729–1745.

[13] Fan Z, Wu Y, Zhao X, Lu Y. Simulation of polycrystalline structure with voronoi diagram in laguerre geometry based on random closed packing of spheres. *Computational materials science* 2004; **29**(3):301–308.

[14] Kanaun S, Tkachenko O. Mechanical properties of open cell foams: Simulations by laguerre tesselation procedure. *International Journal of Fracture* 2006; **140**(1-4):305–312.

[15] De Cola F, Bombace N, Falco S, Petrinic N. Concurrent adaptive mass-conserving comminution of granular materials using rigid elements. *Proceedings of the 7th International Conference on Discrete Element Methods*, *Springer Proceedings in Physics*, vol. 188, Springer: Singapore, 2017.

[16] Kumar S, Kurtz SK. Simulation of material microstructure using a 3d voronoi tesselation: Calculation of effective thermal expansion coefficient of polycrystalline materials. *Acta metallurgica et materialia* 1994; **42**(12):3917–3927.

[17] Fritzen F, Böhlke T, Schnack E. Periodic three-dimensional mesh generation for crystalline aggregates based on voronoi tessellations. *Computational Mechanics* 2008; **43**(5):701–713.

[18] Falco S, Siegkas P, Barbieri E, Petrinic N. A new method for the generation of arbitrarily shaped 3d random polycrystalline domains. *Computational Mechanics* 2014; **54**(6):1447–1460.

[19] Falco S, De Cola F, Petrinic N. A method for the generation of 3d representative models of granular based materials. *International Journal for Numerical Methods in Engineering* 2016; (submitted).

[20] Si H. Tetgen, a delaunay-based quality tetrahedral mesh generator. *ACM Transactions on Mathematical Software (TOMS)* 2015; **41**(2):11.

[21] Duan Q, Kroese DP, Brereton T, Spettl A, Schmidt V. Inverting laguerre tessellations. *The Computer Journal* 2014; :bxu029.

[22] Lautensack C. Fitting three-dimensional laguerre tessellations to foam structures. *Journal of Applied Statistics* 2008; **35**(9):985–995.

[23] Chiu SN, Stoyan D, Kendall WS, Mecke J. *Stochastic geometry and its applications*. John Wiley & Sons, 2013.

[24] De Cola F, Falco S, Barbieri E, Petrinic N. New 3d geometrical deposition methods for efficient packing of spheres based on tangency. *International Journal for Numerical Methods in Engineering* 2015; :1–24.

[25] Barber CB, Dobkin DP, Huhdanpaa H. The quickhull algorithm for convex hulls. *ACM Transactions on Mathematical Software (TOMS)* 1996; **22**(4):469–483.

[26] Schneider CA, Rasband WS, Eliceiri KW, *et al.*. Nih image to imagej: 25 years of image analysis. *Nat methods* 2012; **9**(7):671–675.

[27] Mendelson MI. Average grain size in polycrystalline ceramics. *Journal of the American Ceramic Society* 1969; **52**(8):443–446.

[28] Wurst J, Nelson J. Lineal intercept technique for measuring grain size in two-phase polycrystalline ceramics. *Journal of the American Ceramic Society* 1972; **55**(2):109–109.

[29] Fleming P. Computer aided design of regulators using multiobjective optimization. *Annual Review in Automatic Programming* 1985; **13**:47–52.